Journal of Sound and Vibration 446 (2019) 195–210

Contents lists available at ScienceDirect

Journal of Sound and Vibration

journal homepage: www.elsevier.com/locate/jsvi

Influence of soil characteristics on natural frequency-based bridge scour detection

Ting Bao [a, *], Zhen Leo Liu [b, **], Kelsey Bird [c]

[a] Research Associate, Department of Civil and Environmental Engineering, Michigan Technological University, 1400 Townsend Drive, Dow 854, Houghton, MI 49931, USA

[b] Department of Civil and Environmental Engineering, Michigan Technological University, 1400 Townsend Drive, Dillman 201F, Houghton, MI 49931, USA

[c] Undergraduate Research Assistant, Department of Civil and Environmental Engineering, Michigan Technological University, 1700 Townsend Drive, 251 DHH, Houghton, MI 49931, USA

A R T I C L E I N F O

Article history:
Received 4 December 2017
Received in revised form 5 January 2019
Accepted 22 January 2019
Available online 23 January 2019
Communicated by: G. Degrande

Keywords:
Predominant natural frequency
Scour detection
Soil characteristics
Soil elastic modulus
Winkler model

A B S T R A C T

The concept of detecting scour severity by analyzing the change in the Predominant Natural Frequency (PNF) of a bridge pier has been gaining increasing interest in recent years. Previous studies primarily focus on this topic using less cohesive soils such as highly erodible sands, whereas no discussions have been reported on the influence of soil characteristics, especially those of cohesive soils, on the PNF. This missing knowledge gap is critical for this application as cohesive soils are an essential part of the soil-pier interaction to determine PNFs. This study aims to fill this knowledge gap by investigating three issues that are related to soil characteristics: 1) the effect of soil types on the PNF variation; 2) the questionable issue regarding the pier diameter effect for soil-pier dynamic modeling using the Vesic analytical expression; and 3) contradictory statements in the existing studies regarding the influence of the soil's elastic modulus on the PNF variation. For the purpose, a series of lab-scale tests is first conducted, and a Winkler-based numerical model is then developed and validated against the experimental results to investigate the effect of soil characteristics on the PNFs measured from systems with cohesive soils and those with less cohesive soils. We found that the soil characteristics affect the PNF by providing a different lateral stiffness to the soil-pier interaction. The strength of the soil-pier interaction mainly depends on the lateral stiffness of each type of soils. In-depth discussions are also made to clarify the pier diameter effect on the predicted PNFs from both less cohesive and cohesive soils. It was clarified that the distribution of the soil's elastic modulus determines whether the pier diameter effect needs to be considered using the Vesic analytical expression. Further simulations are finally conducted with more complex and realistic field soil conditions to mediate the contradictory statements regarding the influence of the soil's elastic modulus. The simulation results indicated that the soil's elastic modulus significantly influences the PNFs. The PNF variations differ under different elastic moduli of soils and distributions of elastic moduli with soil depths.

* Corresponding author.
** Corresponding author.
E-mail addresses: tbao@mtu.edu (T. Bao), zhenl@mtu.edu (Z.L. Liu), kmbird@mtu.edu (K. Bird).

https://doi.org/10.1016/j.jsv.2019.01.040
0022-460X/

1. Introduction

Scour around bridge foundations is a major threat to bridge safety for inducing bridge failures [1,2], which severely impacts the service to road users. As reported by Yu et al. [3], over 20,000 bridges in the United States are subjected to deficiencies resulting from critical scour issues. Among them, more than 870 scour-induced bridges collapsed in the past 40 years [4] and, many bridges are in danger of failures resulting from scour, leading to the enormous financial cost for bridge repairs and retrofitting. Furthermore, scour-related catastrophes greatly endanger human lives as scour-induced bridge collapses occur suddenly without prior warnings. Such concerns lead to the momentum in the prevention of scour issues.

Numerous efforts have been made to estimate the critical scour depth. The traditional way to evaluate scour depths is to install underwater instruments near bridge foundations such as sonar devices [5] and tethered buried switches [6]. Such instruments can detect information regarding a certain scour depth if a scour hole reaches the critical depth. Unfortunately, various challenges exist in the efficiency, reliability, durability, and cost-effectiveness of these instruments to provide continuous information on the scour evolution, which is of great significance to bridge safety against scour-induced bridge collapses. To address this problem, several new sensors have been developed for continuous scour monitoring. The mechanisms of these sensors, which allow for monitoring of bridge scour, include measuring the changes in the reflected ultrasonic pulses between water and soils [7], reading the disturbances of rocks with different IDs to the Earth's magnetic field [8,9], detecting the large differences between the dielectric properties of water and sediments in the time domain signals [3,10], analyzing the received signal's strength in the reflected acoustic beams measured from soil deposits [11], etc. The observed data confirmed that these techniques can provide continuous information on the scour progression for monitoring certain sour conditions. Even though those traditionally and recently developed sensors for scour detection can measure scour depths directly and continuously, they give no further information on the health condition of a bridge caused by the current scour depth because of a gap between them.

A novel way to detect scour severity based upon vibration has been attracting increasing research attention in recent years. This novel approach is possibly the most feasible and applicable way for long-term bridge scour monitoring by providing real-time and critical information on the health condition of a bridge. The hypothesis of this approach is that scour has an effect on the frequency spectrum of a bridge or a bridge component, such as a pier. To explore this concept, numerical simulations have been conducted to investigate the relationship between the Predominant Natural Frequency (PNF) and scour depths [12–15]. The simulation results have verified that the PNF of a bridge pier decreases with scour progression. In addition to the simulations, both laboratory tests [16] and field tests [17] have confirmed that the PNF decreases as a scour hole develops. Efforts have also been made to provide an in-depth understanding regarding the effectiveness of the PNF-based scour detection approach on different types of foundations [16,18] and on ambient vibration measurements [16,19], useful schemes for data post-processing [19,20], and influence of the fluid-structure interaction [21]. Further progress to advance this scour detection method has also been made by investigating the optimal location for sensor installations [22], and discussing the PNFs measured from symmetrical and unsymmetrical scour holes [22]. One recent contribution for the topic is that Prendergast and Gavin [23] compared five widely used formulations of the initial stiffness with experimental results and concluded that the Vesic [24] analytical equation is more accurate for soil-pier dynamic Winkler modeling. Most recently, a bespoke vehicle-bridge-soil interaction model was developed to detect scour based on the PNF using a moving vehicle [15,25]. The results reported by Prendergast et al. [15] showed that the magnitude of changes in the PNF is sufficiently large for scour severity monitoring and also confirmed that moving vehicles can generate realistic dynamic signals for obtaining the PNF for scour monitoring.

Despite the above progress, there are still three unclear issues that are related to soil characteristics in the framework of the PNF-based scour detection approach. First, there have been no discussions on the effect of soil types on the PNF variation, though soils are an essential part of the framework of this application. Most conventional tests were performed with lab-scale models in a flume using less cohesive soils, such as highly erodible sands [16,17], due to time and economic constraints. However, cohesive soils such as clays are an essential part of the soil-pier interaction. In fact, many floodplains, where most bridge foundations are located, are composed of less erodible soils [26]. Field measurements reported by Mueller and Wagner [27] also showed that cohesive soils are the bed materials for many real bridges, of which many piers, e.g., a real bridge pier in Texas, are subjected to serious scour issues (scour depth over 7.1 m). The properties and behavior of these materials are thus critical to the soil-pier interaction for those real bridges, and as a result, may alter the way that the PNF varies as scour develops. Second, the pier diameter effect is still questionable [28] for soil-pier dynamic modeling using the Vesic [24] analytical expression. Though Prendergast and Gavin [23] concluded that this analytical expression is more accurate compared to the other four expressions, the pier diameter effect in fact is not considered in Ref. [23] as the modulus of subgrade reaction has no diameter term in the denominator of the original expression [24]. The results from Ling [29] and Carter [30] showed that the pier diameter effect is significant and the results are more accurate if this expression is modified to consider the diameter effect; while the later results from Ashford and Juirnarongrit [31] indicated that the pier diameter effect is insignificant and the results obtained using this expression directly are more accurate. This controversy, which in fact is greatly influenced by soil characteristics (see details in Section 3.3), needs to be clarified. Third, contradictory statements have been made in the existing studies regarding the influence of the soil's elastic modulus on the PNF variation [32]. The numerical results from Huang's model [33] indicated that the soil's elastic modulus has a negligible impact on the PNF; while the numerical results from Zhang's model [18] showed that the numerical PNFs are significantly different if the elastic moduli are different. The soil's elastic modulus is an important mechanical property of all types of soils to determine soil stiffness for the soil-pier interaction. Therefore, such contradictory statements need to be investigated to understand the influence of the soil's elastic modulus in the PNF-based scour detection approach.

To advance the topic, this study aims to investigate the influence of soil characteristics, especially those of less erodible soils, on the PNF with a focus on the soil-pier interaction. The main objective is to resolve the above three issues related to soil characteristics. In Section 2.1, a series of lab-scale tests is conducted with an open-ended pier embedded in a less cohesive soil and a cohesive soil. A Winkler-based numerical model is developed in Section 2.2 and validated against the experimentally measured PNFs in Section 3.2 to understand the soil-pier interaction provided by the cohesive and less cohesive soils. Critical discussions regarding the pier diameter effect for soil-pier dynamic Winkler modeling are made in Section 3.3 for two lateral stiffness determination methods. The diameter effect on the predicted PNFs from both less cohesive and cohesive soils using the Vesic [24] analytical expression is clarified based on the published data and the results obtained in this study. Further simulations with more complex and realistic field soil conditions are conducted in Section 3.4 to mediate the contradictory statements in the existing studies regarding the influence of the soil's elastic modulus on the PNF.

2. Methods

2.1. Lab-scale test

2.1.1. Testing description

A typical approach of PNF-based scour detection is to install a sensor on a bridge pier, either in the laboratory [16,17] or in situ [34], to record the dynamic response in the free vibration of the pier generated by an external force. The change in the PNF can then be obtained by transferring the dynamic data from the time domain into the frequency domain using the Fast Fourier Transform (FFT) [17,35]. The laboratory test conducted by Prendergast et al. [17] using a steel rod as an open-ended pier confirmed the reliability of utilizing the PNF to detect scour progression. The following sensitivity study made by Prendergast and Gavin [36] further validated the applicability of this method for full-scale bridge scour detection. Following the test method used by Prendergast et al. [17], in the current study, a lab-scale model with an open-ended pier was constructed and investigated to assess the dynamic response of a pier embedded into a sand and a clay, respectively. The sand used to consider a less cohesive soil was uniform with the same grading (Fig. 1(a)). The clay utilized to consider a cohesive soil had a medium plasticity collected from a landslide site near a river (Fig. 1(c)). A real pier could have different material properties and geometric configurations. Therefore, four different piers were adopted and embedded into the above two soils. The concrete column and brick were used to simulate bridges with a single column pier and rectangular pier, respectively. The hollow pipe and steel rod were utilized to simulate bridges with steel piers. The soils were housed in a plastic tank with dimensions of 520 mm, 855 mm, and 1280 mm in depth, width, and length, respectively. The soils were compacted layer by layer in an increment of 150 mm, in which the sand was compacted to an approximate 100% relative density.

An accelerometer was mounted at a location that is very close (10 mm) to the top of a pier to record the dynamic response as shown in Fig. 1(a) and (c). To collect dynamic data, the accelerometer and a modal hammer were connected to a data acquisition system as shown in Fig. 1(b). The modal hammer was utilized to generate vibration by applying a transient force onto the plane where the accelerometer was fixed. The system responded instantly when the transient force was applied. Dynamic signals of the pier and the transient force at each impact were recorded by the data acquisition system. This system was established to take data samples at a scanning frequency of 3000 Hz.

The scour process was simulated by removing the soil around the pier. The initial scour level (Level 1) corresponded to the situation of no scour hole around the pier. The scour Level 6 was the final scour depth for each test pier, for which 5 layers of

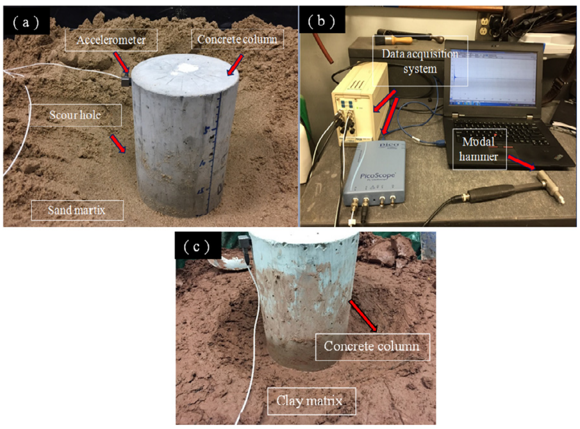

Fig. 1. Components of laboratory scour test: (a) a test pier in the sand, (b) data acquisition system and (c) a test pier in the clay.

soil were removed. An increment in the scour level of 20 mm was used to simulate progressive scour. As explained above, four types of test piers were used. The geometric properties and scour conditions of each pier type are detailed in Table 1. The schematic of the geometry of the test piers is shown in Fig. 2. The simulation results concluded by Ju [21] showed that the difference in the PNFs calculated with and without the fluid-structure interaction was small. Therefore, the effect of the water-pier interaction was assumed to be negligible and not considered in this study. However, water was added into the soil matrix because soils around a bridge pier, in reality, are underwater. The volumetric water contents of the sand and clay matrices are approximately 10.8% and 62.1%, respectively. Under this water content condition, the clay is nearly saturated and therefore, the PNF measured in such the clay can be considered to be close to that of fully saturated clays around bridge piers. PNFs measured in the sand also can be considered to be close to those measured in sands around bridge piers, because the water content has a negligible effect on the major mechanical property of sands [37], i.e., the elastic modulus.

2.1.2. Experimental results

According to Refs. [35,38], it is of great importance to assess the impulse force applied to the pier because the frequency and the duration of the contact between the hammer and the pier could cause negative effects on the measured dynamic signals with noises in the initial portion of the signals. Fig. 3(a) and Fig. 3(b) depict a typical impulse force applied to the pier and its frequency spectrum. The contact duration is less than 2 ms, and an almost constant frequency amplitude from 0 Hz to 500 Hz is maintained within this duration. The impulse force generated in this study can thus be regarded as an ideal impulse as proposed in Ref. [35].

Fig. 3(c) and (d) show the measured dynamic responses of the hollow pipe in terms of acceleration in the sand and clay matrices at scour Level 1 and Level 6. The acceleration contains a significant amount of high frequency vibration including assembled and superposed waveforms due to local effects [17,39]. The aim of this study is to extract the PNF of the pier in the low frequency range to identify the scour depth, which is not relevant to those high frequencies. Therefore, a low-pass filter was applied to the signals of acceleration in Fig. 3(c) and (d) to show the difference in the periods between scour Level 1 and Level 6. A similar approach was used in the study of Prendergast et al. [17]. The filtered signals are shown in Fig. 3(e) and (f). The results clearly show that the periods in the filtered signal of scour Level 6 are significantly larger than that of scour Level 1 due to a greater scour depth.

In order to obtain the PNF at each scour level, the FFT was then used to transfer the original dynamic signals rather than the filtered signals from the time domain to the frequency domain. As shown in Fig. 4(a), the PNF of the hollow pipe decreases from 20.5 Hz (Level 1) to 14.2 Hz (Level 6) in the sand matrix. The PNF decreases from 17.6 Hz to 10.5 Hz in the clay matrix. In Fig. 4(b), a similar result was obtained in the frequency spectra of the concrete column, in which the PNF decreases from 130.6 Hz (Level 1) to 51 Hz (Level 6) in the sand matrix and from 37 Hz (Level 1) to 19.2 Hz (Level 6) in the clay matrix. In all of the tests, there is a clear reduction in the PNF regardless of the types of piers and soil media (Fig. 4(c)-4(f)).

Table 1
Geometry of the test piers and initial scour situations.

Test pier	Height (mm)	Width/Length (mm)	Diameter (inner/outer) (mm)	Embedded length (sand/clay) (mm)	Scour Increment (mm)	Soil compactness
Concrete column	306	–	-/153	226/156	20	high
Concrete brick	406	77/100	–	236/166	20	high
Steel rod	1640	–	25	300/250	20	high
Hollow pipe	1610	–	49/51	290/260	20	high

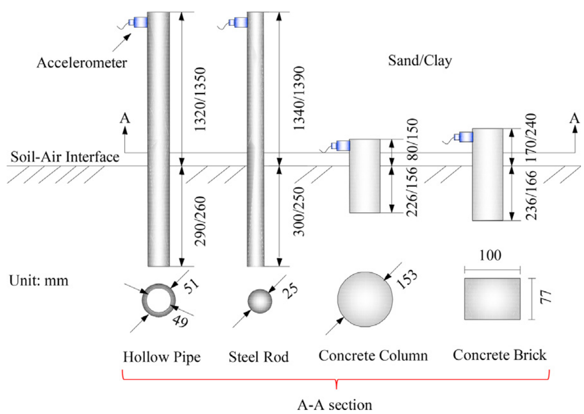

Fig. 2. Schematic of the geometry of test piers.

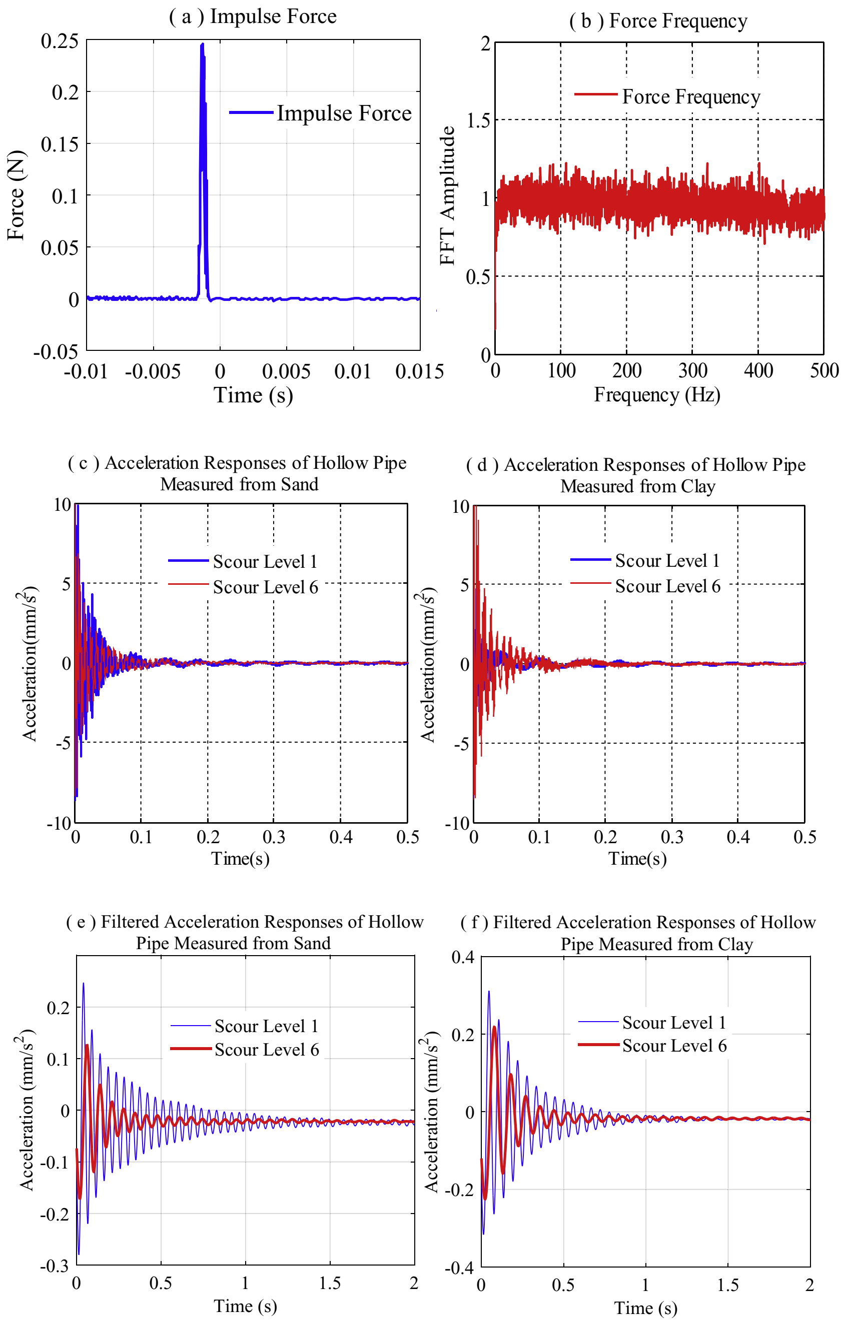

Fig. 3. Collected dynamic signals: (a) an impulse force and (b) its frequency spectrum; acceleration of the pier at scour Level 1 and Level 6 in the (c) sand and (d) clay; filtered acceleration in the (e) sand and (f) clay.

As indicated in Fig. 4(c)–4(f), the change in the PNF variation may depend on the geometries of the test piers. The PNF of the brick (Fig. 4(d)) decreases relatively fast at the beginning when compared to that of the concrete column (Fig. 4(c)) in both the sand and clay matrices. For the concrete column and brick, the PNFs measured in the different soils are different. To be more specific, the range of the PNF response in the sand matrix is considerably larger than that in the clay matrix. This is mainly due to the higher level of interaction with the sand attributed to a high relative density than the level of interaction with the clay. However, PNF variations of the hollow pipe and the steel rod measured in the sand and clay from Fig. 4(e) and (f) seem similar. Unfortunately, those observations are not conclusive and only provide limited insights into the influence of soil characteristics by simply comparing the PNF variations in Fig. 4(c)–4(f). A numerical study is therefore conducted to provide a better understanding of the influence of soil characteristics, which will be discussed in Section 3.2.

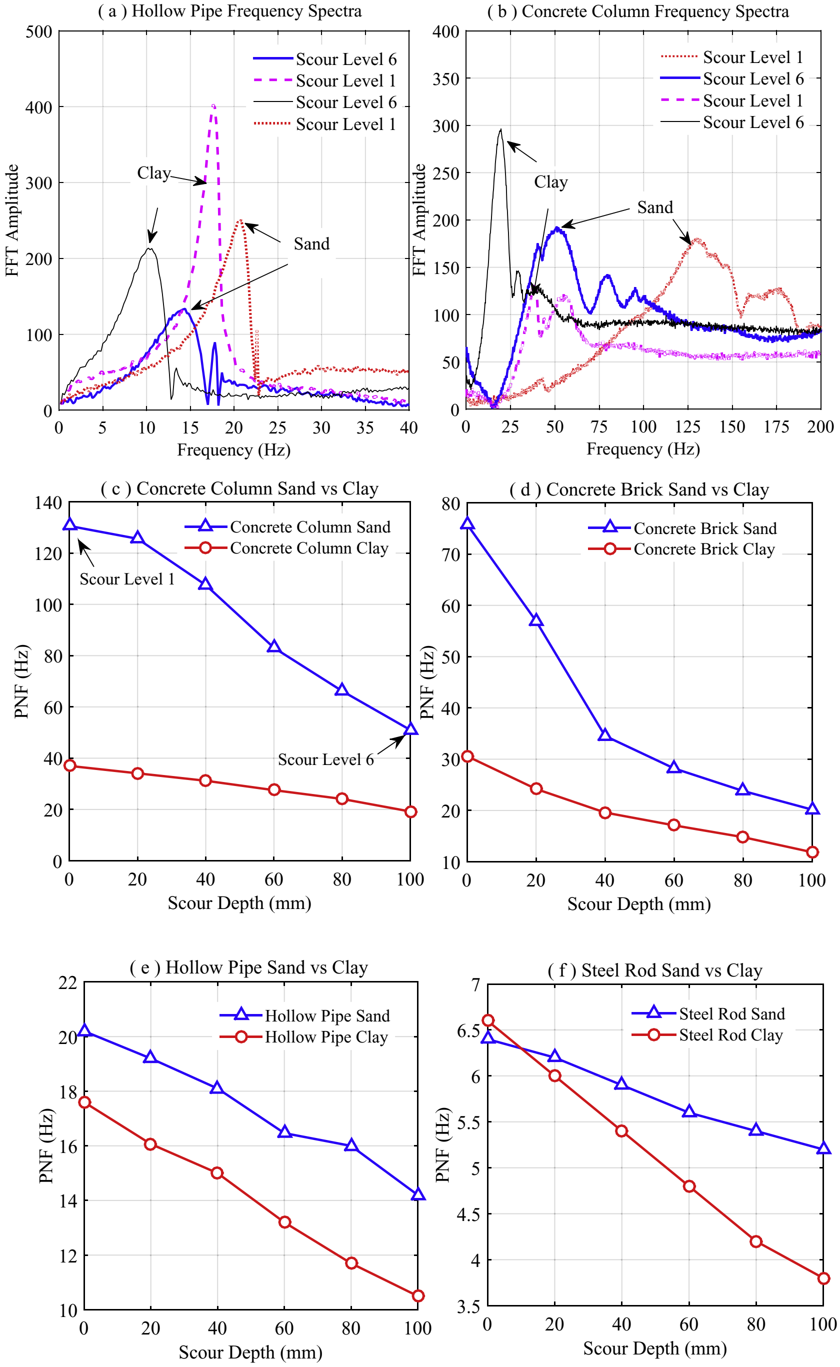

Fig. 4. Measured PNFs: (a) unfiltered PNF spectra of the hollow pipe; (b) unfiltered PNF spectra of the concrete column; (c) PNF variations of the concrete column; (d) PNF variations of the concrete brick; (e) PNF variations of the hollow pipe; and (f) PNF variations of the steel rod.

2.2. Numerical model

2.2.1. Theoretical formulation

In order to investigate the effects of soil characteristics on the PNF, a numerical model based upon the Winkler model was developed to simulate the above lab-scale tests. The hypothesis of the Winkler approach is to model the pier using a series of beam elements and to represent soils as a series of unconnected and concentrated springs perpendicular to the pier [40]. The soil-pier interaction of this model can be easily implemented and yield sensible and good results in foundation engineering practice [40–42]. In this section, the hollow pipe and the steel rod were utilized as a pier in the simulations, in which the lateral spring was considered only without the rotational spring as those were done in the existing literature [29–31,43]. To simulate progressive scour, the springs were gradually removed from the top to the corresponding scour depths in the tests. The numerical models used to model the lab-scale tests are shown in Fig. 5.

The dynamic responses of the model to a given impulse force can be calculated with the dynamic equation of motion as shown below [44].

$$[\mathbf{M}]\ddot{\mathbf{x}} + [\mathbf{C}]\dot{\mathbf{x}} + [\mathbf{K}]\mathbf{x} = \mathbf{F} \tag{1}$$

where $[\mathbf{M}]$, $[\mathbf{C}]$ and $[\mathbf{K}]$ are symmetric matrices for the mass, damping and stiffness, respectively; $\mathbf{x}$ is the displacement vector; $\ddot{\mathbf{x}}$ and $\dot{\mathbf{x}}$ are the acceleration and velocity vectors, respectively; and $\mathbf{F}$ is the external force vector. In this study, the modal analysis was adopted to compute the natural frequency of the system. This method solves Eq. (1) to obtain the natural frequency of the beam partially embedded in the soil by analyzing the linear undamped free vibration of that beam. Based on this, Eq. (1) can be simplified to

$$[\mathbf{M}]\ddot{\mathbf{x}} + [\mathbf{K}]\mathbf{x} = 0 \tag{2}$$

The general solution to Eq. (2) can be assumed of the form, $x(t) = Ue^{i\omega t}$, where ω is the angular natural frequency of the beam and U is the modal shape function. Substituting this solution into Eq. (2), we can obtain

$$\left([\mathbf{M}] - \omega^2[\mathbf{K}]\right)U = 0 \tag{3}$$

Eq. (3) is an eigenvalue problem that can be solved to obtain ω. Then, the natural frequency of the beam, f, can be computed simply using $f = \omega/2\pi$. To compute the natural frequency in the modal analysis, the program was developed with the assistance of MATLAB.

2.2.2. Soil stiffness determination for winkler spring

The stiffness of springs is crucial in correctly modeling the behavior of the soil-pier interaction. To satisfactorily represent the lateral stiffness of soils around the test piers, the Small-Strain Stiffness Method (SSSM) and the American Petroleum Institute Method (APIM) were used in this study as both can yield the good lateral spring stiffness of soils to a pier in which the predicted PNFs are close to the measured ones according to Ref. [17].

2.2.2.1. APIM stiffness for sands. According to the API design code [45], the APIM uses the load-deflection (p-y) curves of different types of soils to provide the lateral stiffness, in which the lateral stiffness of sands can be easily estimated as the API code provides the initial subgrade reaction curves with respect to the relative density of sands based on the p-y curves [45]. The lateral soil p-y relationship for sands is [45]:

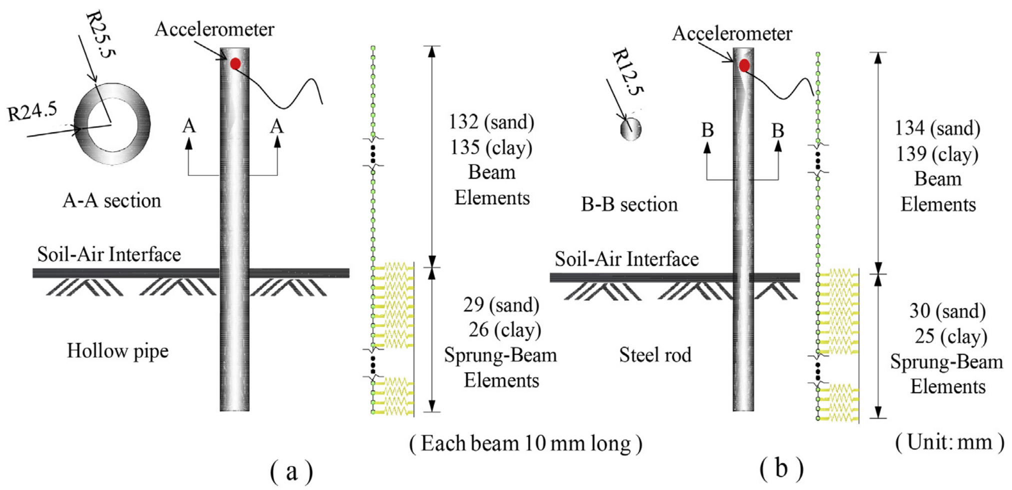

Fig. 5. Schematic of discrete springs spaced along the test piers and its dimensions for simulations of: (a) the hollow pipe and (b) the steel rod.

$$p = Ap_u \tanh\left[\frac{kH}{Ap_u} y\right] \tag{4}$$

where p is the lateral load per unit length of a pier (kN/m); y is the lateral deflection (m); A is the factor to account for a cyclic or static loading condition; p_u is the ultimate bearing capacity at a certain soil depth of H (kN/m); and k is the initial modulus of subgrade reaction (kN/m^3) which can be determined with the relative density of sands. Since a lateral impulse force impacting a pier within a very short duration induces very small strains in the sand mass, the dynamic responses of the sand mass on the sand-pier boundary can be represented by differentiating Eq. (4) at $y = 0$ [17]:

$$\frac{dp}{dy} = \frac{Ap_u \frac{kH}{Ap_u}}{\cosh^2\left(\frac{kH}{Ap_u} y\right)}\Big|_{y=0} = kH \tag{5}$$

The lateral stiffness of sands of the soil-pier interaction is given by multiplying kH in Eq. (5) by the spacing between adjacent springs at discrete locations along the pier.

2.2.2.2. SSSM stiffness for sands and clays. The lateral stiffness of soils in terms of the SSSM is typically associated with strains of a small order as lateral dynamic loading causes small strains in a soil mass [46]. The critical parameter for dynamic analyses on the small strain level is the elastic modulus E_0. The distribution of this modulus in the soil stratum can also reflect the effective overburden pressure of realistic soil conditions via the overburden correction factor of the Standard Penetration Test (SPT) [29]. The geophysical method [47] was used to assess E_0 of the soils used in the laboratory tests for the simulations. As shown in Fig. 6, two metal columns were embedded into the soil matrix at a certain wave propagation distance. The velocity of compression waves in the soil matrix was calculated by measuring the difference between the arriving times at the impact point and the point at which the signal was received using an accelerometer. E_0 in most cases varies with the soil depth. However, in this study, E_0 was assumed to be uniformly distributed within the soil matrix because the soil used in the laboratory tests was compacted uniformly. The velocity of a compression wave in the sand and clay matrices are estimated to be 213 m/s and 216 m/s, respectively.

The soil's elastic modulus E_0 can then be computed using the following expression [47]:

$$E_0 = \frac{\rho V_c^2 (1+\nu)(1-2\nu)}{1-\nu} \tag{6}$$

where v is the small strain Poisson's ratio of soils; V_c is the compression wave velocity (m/s); and ρ is the total mass density of soils (kg/m^3), which was estimated using the sand-cone method according to ASTM D1556.

According to Ref. [31], the lateral spring stiffness can be determined by multiplying the modulus of subgrade reaction K (kN/m^2) by the spacing of the adjacent springs. The relationship between K and the material properties in an elastic continuum in terms of the Winkler spring model is given by Eq. (7):

$$K = \frac{1.0E_0}{1-\nu^2}\left[\frac{E_0 D^4}{E_p I_p}\right]^{1/12} \tag{7}$$

where D is the pier diameter (m); and $E_p I_p$ is the flexural rigidity of the pier (kN m^2).

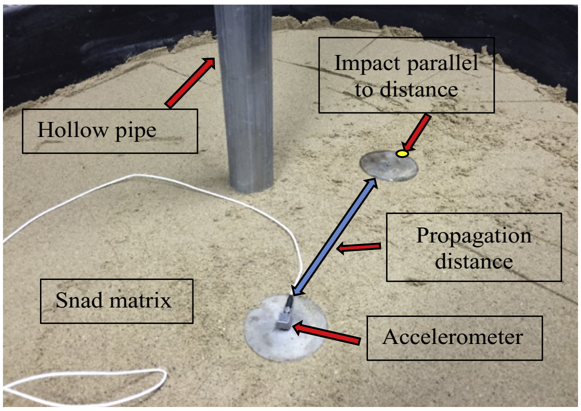

Fig. 6. Geophysical methods for E_0 measurements.

3. Results and discussions

In this section, the numerically computed PNFs are validated against the experimentally measured PNFs. Discussions regarding the pier diameter effect are made for the two stiffness determination methods. Further discussions are also made based on more complex and realistic field soil conditions to mediate the contradictory statements regarding the influence of the soil's elastic modulus on the PNF.

3.1. Stiffness derived from SSSM and APIM

The lateral stiffness of soils for the lab-scale tests is shown in Fig. 7. For the hollow pipe, the lateral stiffness of both the sand and clay is uniform along the hollow pipe in the SSSM, while the lateral stiffness obtained by the APIM linearly increases with soil depths. It can be clearly seen that the APIM stiffness is much lower than the SSSM stiffness, which may make the default APIM fail to reflect the real situation of the tests. The reason for this inappropriate distribution is that the sands used in the laboratory were compacted to an approximate 100% relative density. However, the initial modulus of subgrade reaction k, by default in the APIM, was estimated at a relative density of 80%, which thus underestimates the stiffness of soils used in the tests.

To provide a better estimation of stiffness, the APIM stiffness was modified by multiplying the initial modulus of subgrade reaction k by 3. The reason for this is that the APIM stiffness should be comparable to the SSSM stiffness, because the SSSM stiffness is computed based on the parameters of the soils tested experimentally. After this modification, the average of the modified APIM stiffness is then comparable to that of the SSSM stiffness (Fig. 7(a)). For the steel rod, the lateral stiffness of both the sand and clay derived from the SSSM is uniformly distributed along the axial direction of the steel rod as shown in Fig. 7(b). The modification was then made using an identical procedure to that used for the hollow pipe to obtain the appropriate APIM-based stiffness.

3.2. Comparison between measured and computed PNFs

The numerically computed PNFs of the hollow pipe and the steel rod were compared with the experimentally measured PNFs in both the sand and clay matrices. As can be seen in Fig. 8(a), the variation of the PNF with scour depths of the hollow pipe in both the sand and clay using the SSSM-based lateral stiffness agree well with the experimental data. However, the APIM-based PNF seem to be overestimated in a large scour depth range because soils provide higher values of the APIM-based lateral stiffness in a large scour depth range than those in a small scour depth range.

The computed PNFs of the steel rod are slightly higher than the measured PNFs in both the sand and clay as shown in Fig. 8(b). This slight error in the numerically computed PNFs is due to the fact that the experimentally measured PNFs were underestimated during the test. This is because the embedded length of the steel rod is too small when compared to its total length and consequently, the free vibration frequently generated by the modal hammer led to a small gap between the soil and the steel rod at locations close to the soil surface, resulting in low values of the measured PNFs. However, the springs used to simulate soils around the pier interact with the pier in an ideal condition, leading to higher values of the computed PNFs than the measured PNFs.

To investigate the effect of soil characteristics, it is also helpful to compare the PNF with respect to soil types. For the hollow pipe in Fig. 8(a), the PNF in the sand matrix is larger than the corresponding values in the clay matrix for the same embedded length. A similar result for the steel rod can also be found in Fig. 8(b). Additionally, this phenomenon was also

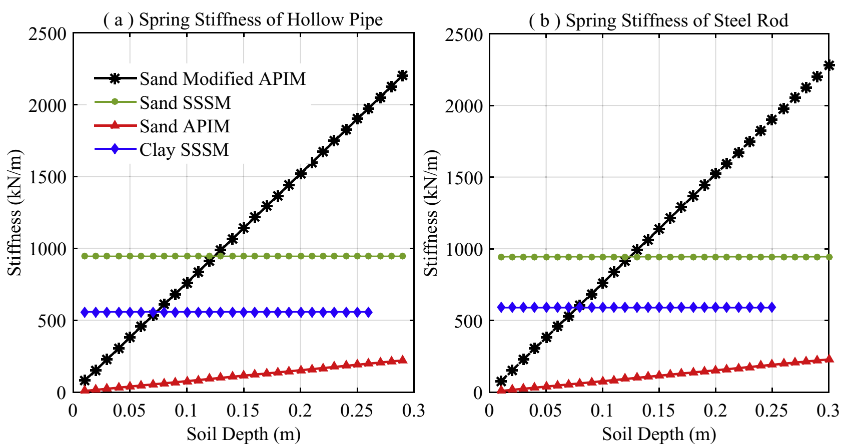

Fig. 7. Stiffness of springs for numerical simulations with: (a) the hollow pipe and (b) the steel rod.

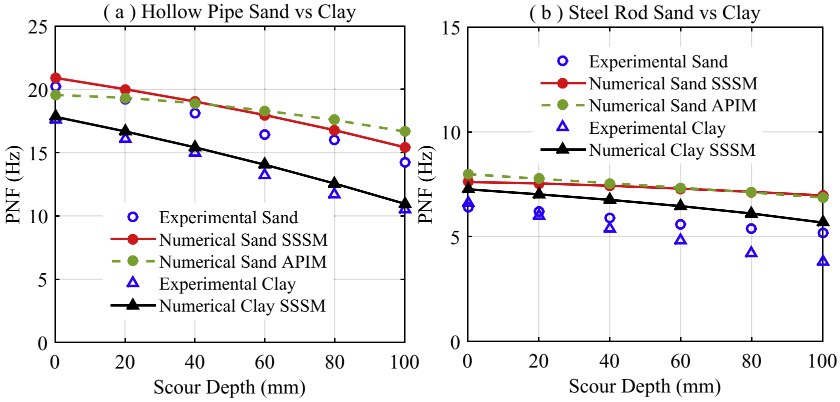

Fig. 8. Comparison between numerical and experimental PNFs.

observed in the tests with the other pier types, i.e., the concrete column and brick presented in Fig. 4. The reason for this phenomenon is that the piers involve a higher level of interaction with the sand than the level of interaction involved with the clay in the tests due to the very high relative density of the sand. In essence, the soil characteristics affect the PNF by providing a different lateral stiffness to the soil-pier interaction. Therefore, for real bridge conditions, the soil type can serve as an indirect factor. The lateral stiffness of each type of soils plays a dominant role in the PNF by means of determining how strong the soil-pier interaction is.

3.3. Discussions on the applicability of winkler model regarding pier diameter effect

In this section, the pier diameter effect is discussed for the APIM and the SSSM separately.

For the SSSM, the pier diameter effect is considered in Eq. (7), i.e., the Vesic analytical expression. However, the term with the pier diameter has the power of 1/12 and thus, this term is very close to 1.0 for most piers. Furthermore, the pier diameter D in this term will be canceled out for most piers with a circular or a square shape, because the moment of inertia of the pier I_p also has the fourth power of the pier diameter or width. Therefore, the modulus of subgrade reaction is independent of the pier diameter in Eq. (7). However, the results shown in Fig. 9 from ten series of lateral load tests on piers embedded both in sands and clays indicate a significant pier diameter effect [29]. To reduce the deviation, Carter [30] suggested adding a ratio between the pier diameter and a reference diameter to Eq. (7)

$$K = \frac{1.0E_0}{1-\nu^2}\frac{D}{D_{\mathrm{ref}}}\left[\frac{E_0 D^4}{E_p I_p}\right]^{1/12} \tag{8}$$

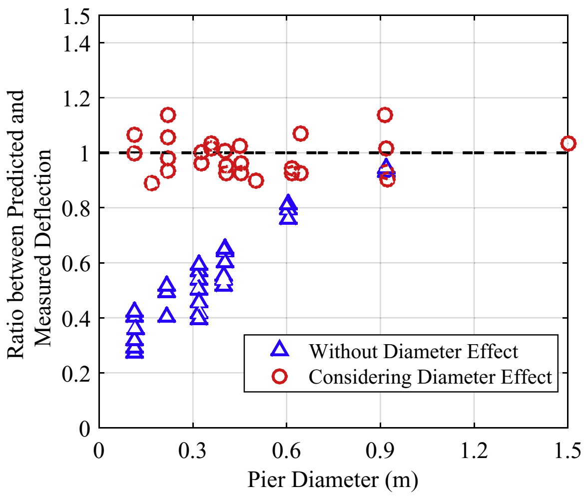

Fig. 9. Result comparisons to consider pier diameter effect using the SSSM with Eq. (7) and Eq. (8) [data adopted from Ref. [29]].

where D_{ref} is 1.0 m. Eq. (8) uses the linear relationship between D and K to reduce deviations. As can be seen in Fig. 9, the ratio between measured results and predicted ones tends to be close to 1.0 using Eq. (8).

Different results [31] in Fig. 10 show that the predicted PNFs of the piers with varied diameters using Eq. (7) are more accurate than those using Eq. (8) when compared to the measured PNFs. This seems contradictory to the results in Fig. 9. In fact, the original form of Eq. (7) is derived based on the soil with a constant E_0 [24]. The pier diameter effect is thus insignificant when the dynamic active length of piers is embedded in the soil with a constant E_0 [48]. The dynamic active length L in soil layers can be calculated by Ref. [49].

$$L = 2D\left(\frac{E_p}{E_0}\right)^{1/4} \tag{9}$$

Though two stratified soil layers with different E_0 values are considered in Fig. 10 [31], the calculated active length is fully located within the first soil layer. Therefore, the predicted PNFs of the piers in Ref. [31] should be similar to those obtained from the first soil layer with the constant E_0.

For the laboratory tests in this study (see Fig. 8), the pier diameter effect is also insignificant because we use the sand and clay with constant E_0 values. As can be seen in Fig. 11, there are significant deviations for the hollow pipe in either the sand or the clay if the pier diameter effect is considered. This further indicates that the pier diameter is insignificant and it is more accurate to use Eq. (7) directly if a pier or the active length of that pier is embedded in soils with a constant E_0. According to Ref. [48], the pier diameter effect will become significant if the active length is embedded in soils having an increasing E_0 with soil depths. The reason for the results shown in Fig. 9 is that the distribution of E_0 in the soils increases with depths. Therefore, the distribution of E_0 in the soil strata is very critical for determining whether the pier diameter effect needs to be considered or not for the SSSM.

The APIM used in Section 3.2 excludes the effect of pier diameters (see Eq. (5)). This assumption is reasonable for the test piers adopted in this study, because a small lateral impulse force impacting the piers induces the “very small” [28] deflection range. In this range, the initial modulus of subgrade reaction k is almost a constant [28]. Good predicted results for sands can also be observed from the study [17] without the pier diameter effect. However, this assumption is not valid for piers in the “relatively small” or “large” [28] deflection ranges under loads, because the initial stiffness of lateral springs is dependent on the geometry of piers in these ranges [28]. For PNF-based scour detection, the magnitude of loads to obtain PNFs is small, but it is still difficult to determine if the pier deflection range of vibration is “very small” or “relatively small” according to the classification in Ref. [28]. Because the deflection range depends on the sand condition, i.e., relative densities and friction angles, e.g., the “very small” deflection range is less than 2.54 mm in the sand condition in Ref. [28]. Essentially, the lateral resistance provided by sands, i.e., the elastic modulus, plays a significant role. Therefore, the pier diameter effect could be neglected for bridge piers with vibration in the “very small” deflection range, but needs to be considered beyond that range. To consider the pier diameter effect in sands, four typical formulations to modify the original APIM are summarized in Table 2. These modified formulations use a reference diameter to reduce the deviation caused by excluding the pier diameter effect. Comparisons of these formulations with numerical results are detailed in Ref. [50], and the accuracy of each formulation varies with load magnitudes [50]. In addition, the lateral stiffness used in the APIM can be obtained by translating the values calculated using 3-dimensional soil-pier modeling based on in-situ soil conditions [43,51], so that the pier diameter effect and

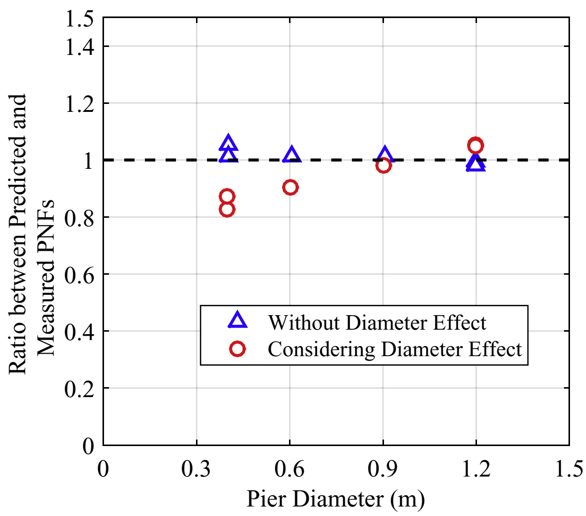

Fig. 10. Result comparisons to consider the pier diameter effect using the SSSM with Eq. (7) and Eq. (8) [data adopted from Ref. [31]].

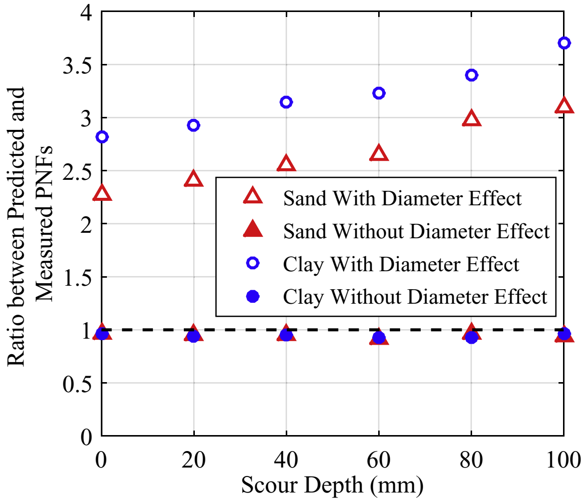

Fig. 11. Comparisons of ratios between the measured and predicted PNFs using Eq. (7) and Eq. (8) for the hollow pipe.

Table 2
Modified formulations to the initial modulus of subgrade reaction for sands.

Reference	Formulation	Parameter	Modification
Wiemann et al. [52]	$k\left(\frac{D_{\mathrm{ref}}}{D}\right)^{\frac{4(1-a)}{4+a}}$	$a = 0.5 \sim 0.6$ $D_{\mathrm{ref}} = 0.61$ m	pier diameter D
Sørensen et al. [53]	$a\frac{1}{H}\left(\frac{H}{H_{\mathrm{ref}}}\right)^{b}\left(\frac{D}{D_{\mathrm{ref}}}\right)^{c}\varphi^{d}$	$a = 50$ MPa $H_{\mathrm{ref}} = 1$ m, $D_{\mathrm{ref}} = 1$ m $b = 0.6,\ c = 0.5,\ d = 3.6$	D; soil depth H; and angle of internal friction φ
Sørensen [54]	$a\frac{1}{H}\left(\frac{H}{H_{\mathrm{ref}}}\right)^{b}\left(\frac{D}{D_{\mathrm{ref}}}\right)^{c}\left(\frac{E_0}{E_{\mathrm{ref}}}\right)^{c}$	$a = 1$ MPa, $E_{\mathrm{ref}} = 1$ MPa $H_{\mathrm{ref}} = 1$ m, $D_{\mathrm{ref}} = 1$ m $b = 0.3,\ c = 0.5,\ d = 0.8$	D; H; and soil's elastic modulus E_0
Kallehave et al. [55]	$k\frac{1}{H}H_{\mathrm{ref}}\left(\frac{H}{H_{\mathrm{ref}}}\right)^{m}\left(\frac{D}{D_{\mathrm{ref}}}\right)^{0.5}$	$m = 0.6,\ H_{\mathrm{ref}} = 2.5$ m $D_{\mathrm{ref}} = 0.61$ m	D and H

soil conditions are considered by the values translated to the APIM. Therefore, these methods can be reasonably adopted based on field sand and load conditions.

3.4. *Influence of the elastic modulus on the PNF*

The good comparison between the experimental and the simulation results confirmed what we observed in the experiments and also, in return, validated the developed Winkler-based numerical program. The influence of the soil's elastic modulus and the significance of the distribution of the soil's elastic modulus for the soil-pier interaction modeling are also exhibited. However, the lab-scale model is not able to reflect the distribution of soil moduli with depths, which could be complicated in reality attributed to the hydrologic and geologic history of the site. In addition to that, contradictory statements, which are proposed in Ref. [32] but not addressed, can be found in the existing studies regarding the influence of the soil's elastic modulus on the PNF variation. That is, the numerical results from Huang's model [33] indicated that the soil's elastic modulus has a negligible impact on the PNF because the different elastic moduli lead to negligible differences in the values of the numerical PNF, as shown in Fig. 12(a). However, a different conclusion was obtained in Zhang's model [18], where the numerical PNFs are significantly different if the elastic moduli are different, as shown in Fig. 12(b). Numerical simulations are conducted to explore the above two issues in this sub-section.

For this purpose, the above validated Winkler-based numerical program for a cylindrical concrete pier with a deck on its top was implemented to consider a simply-supported beam bridge with more complex and realistic field soil conditions according to Refs. [56,57]. This modeling setup considered a variation of the monopile foundation, in which a monoplie and a pier column supported by that monopile were assumed to be a whole homogenous column. 3.6 m beam elements in the air and 11 m sprung beam elements were used. A scour increment of 0.5 m was used in the simulation. The elastic modulus distribution of soils can be determined based upon the field tests of the deep coastal plain sediments where the elastic modulus distributions of both sands and clays are measured and reported in Ref. [58], which confirmed that the soil's elastic modulus is either increasing, uniformly distributed, or decreasing with soil depths. According to Ref. [49], the parabolic increase of E_0 with depths is also common for realistic soil conditions. Based upon the field observations [58] and the parabolic

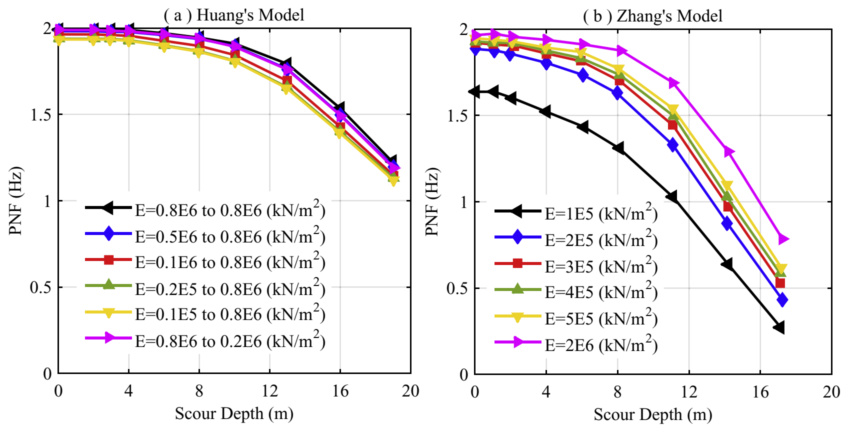

Fig. 12. Comparison between the simulation results from (a) Huang's model [33] and (b) Zhang's model [18] with different soil strengths.

equation [49], four scenarios with different elastic modulus distributions in the soil strata were simulated, i.e., linearly increasing from the top to the bottom, uniformly distributed, linearly decreasing from the top to the bottom, and parabolic increase of E_0 with depths. The model used in the simulation is shown in Fig. 13. A 1.5 m pier diameter was chosen based on real bridge piers with scour issues according to Ref. [27]. The lateral stiffness was derived using the SSSM because this approach is capable for any type of soils, and also can consider the pier diameter effect in terms of the distribution of E_0 with depths. Eq. (7) was used to determine the lateral stiffness for uniformly distributed E_0, i.e., Scenario A in Fig. 13; while Eq. (8) was utilized for the other scenarios, i.e., Scenarios B-D.

As illustrated in Fig. 14(a), the variations of the PNF with scour depths differ at different elastic moduli. The soil with a high elastic modulus provides a very high frequency in the whole scour depth range. An interesting finding is that the influence of the soil's elastic modulus on the PNF is actually significant in the cases analyzed in this study. This is because the lateral stiffness of the soil is dependent on the soil's elastic modulus. A high soil's elastic modulus provides a high lateral stiffness. Also, the rate of the decrease in the PNF is dependent on the soil's elastic modulus. The PNF calculated in the soil with an elastic modulus of 100 MPa decreases faster when compared with that with an elastic modulus of 10 MPa.

The numerical simulations for increasing moduli, decreasing moduli and parabolic increase of moduli with soil depths revealed interesting trends that have not been reported before. For the soil with a linearly increasing elastic modulus, the PNF variations are different under different modulus distributions as shown in Fig. 14(b). The PNF is higher if the elastic modulus of the soil at the bottom is greater, which is due to the larger lateral stiffness provided by the soil with a higher elastic modulus. The PNF obtained based on a linearly increasing elastic modulus is also higher than that obtained using constant E_0 if that constant E_0 is equal to the modulus of the bottom layer in each linearly increasing elastic modulus. This indicates that the PNF mainly depends on the elastic modulus at the bottom. For the soil with a linearly decreasing elastic modulus, the PNF variation is almost the same, especially in a large scour depth range, if the soil's elastic moduli at the bottom are equal (Fig. 14(c)). The PNF obtained using constant E_0 is higher than that obtained based on a linearly decreasing elastic modulus. The main reason is that the PNF is more heavily or even primarily dependent on the distribution of the soil's elastic modulus. This reason can also be supported by the results presented in Fig. 14(d) for the parabolic increase of E_0 with soil depths. The PNFs coincide if the soil's elastic moduli at the bottom are equal. These findings further confirm and detail the conclusions from the lab tests and the numerical simulations in the previous sub-sections: the soil's elastic modulus considerably affects both the absolute value and the variation of the PNF by providing different lateral stiffness to soils around the pier. These

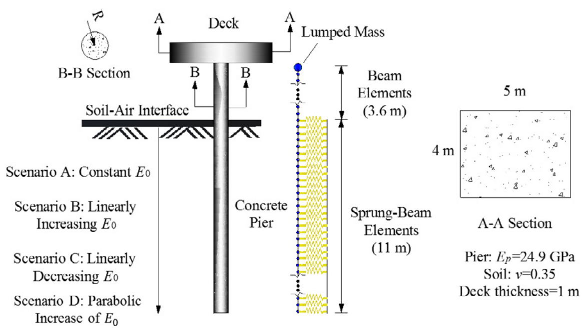

Fig. 13. Schematic of the model used in the simulation.

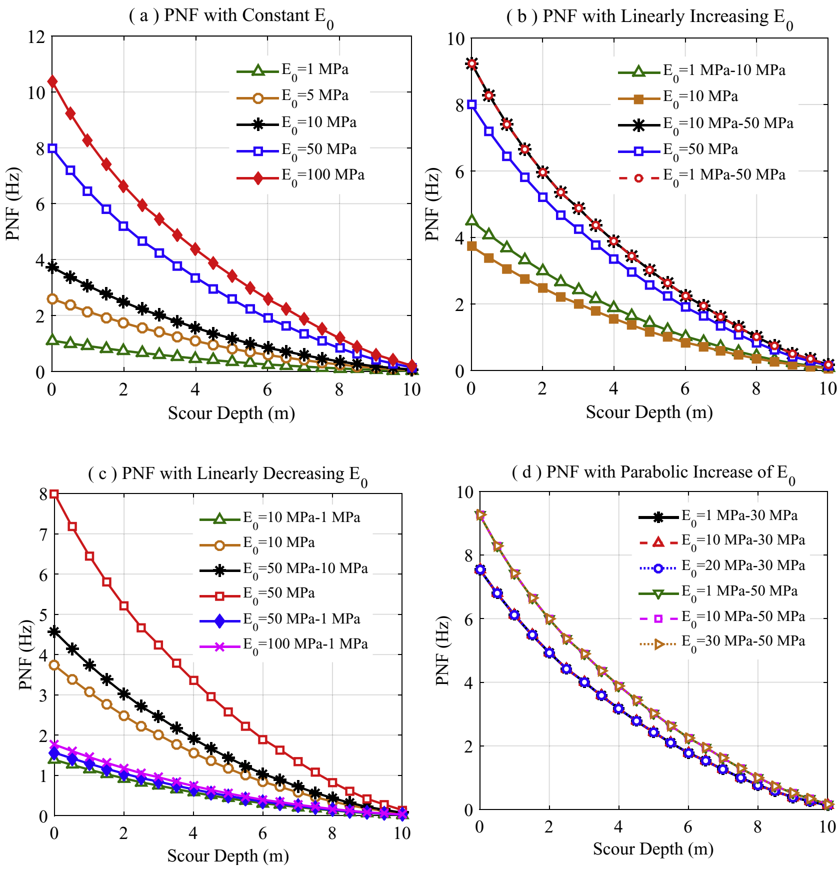

Fig. 14. Numerical PNFs obtained using a pier with 1.5 m diameter: (a) constant E_0, (b) linearly increasing E_0, (c) linearly decreasing E_0 and (d) parabolic increase of E_0.

findings provide valuable insights and guidance for the implementation of the PNF-bridge scour detection method in field conditions including soil characteristics.

4. Conclusions

A series of lab-scale tests with both a cohesive soil (clay) and a less cohesive soil (sand) was performed to investigate the change in the PNFs of varying types of an open-ended pier with different scour severity. A Winkler-based numerical model was developed to investigate the difference in the PNF associated with both the cohesive and less cohesive soils to formulate the soil-pier interaction in numerical simulations. Two methods to determine the stiffness of soils were used for the cohesive soil or the less cohesive soil. The numerically computed results were validated against the experimentally measured results for mutual validation. Discussions regarding the pier diameter effect in the soil-pier dynamic Winkler modeling was made. Further simulations were conducted to mediate the contradictory statements in the existing studies regarding the influence of the soil's elastic modulus on the PNF with more complex and realistic field soil conditions.

The experimental and numerical results indicated that the ranges of the PNF of the test piers in the cohesive soil and the less cohesive soil are different. The primary reason is that the soil characteristics affect the PNF by providing different lateral stiffness to the soil-pier interaction. The lateral stiffness of each type of soils, which determines the strength of the soil-pier interaction, depends on its elastic modulus for dynamic analyses on a small strain level. The key focus for future scour prediction thus could be on the determination of the soil's elastic modulus in the strata. The soil type can serve as an indirect factor, which affects the PNF via the elastic modulus.

Discussions regarding the pier diameter effect showed that soil characteristics play a significant role in the consideration of this effect. For the APIM, the pier diameter effect could be neglected for bridge piers with vibration in the "very small" deflection range, but needs to be considered beyond that range. This deflection range mainly depends on the lateral resistance of sands. For the SSSM, the results in this study further confirmed that the pier diameter is insignificant if a pier or its active length is embedded in the soil with a constant elastic modulus. If the active length is embedded in the soil with a variable elastic modulus, e.g., an increasing elastic modulus with soil depths, the pier diameter effect needs to be considered.

The PNF variations differ at different elastic moduli of soils. For uniformly distributed soil's elastic moduli, a soil with a high elastic modulus leads to a very high frequency in the whole scour depth range due to its higher lateral stiffness. The rate of decrease in the PNF is also dependent on the soil's elastic modulus. The PNF calculated in the soil with a high elastic modulus decreases faster when compared to that with a low elastic modulus. These results mediate the contradictory statements in the existing studies.

For the soil with linearly increasing elastic moduli with soil depths, the PNF is higher if the elastic modulus of soils at the bottom is higher. However, the PNF variation with either linearly decreasing elastic moduli or the parabolic increase of moduli is almost the same if the soil's elastic moduli at the bottom layer are equal. The main reason is that the PNF may be more heavily or even primarily dependent on the elastic modulus of the soil at locations very close to the bottom. This is the first time these interesting patterns were revealed, which could serve as a guideline for the application of PNF-based scour detection in field conditions including soil characteristics.

References

[1] K. Wardhana, F.C. Hadipriono, Analysis of recent bridge failures in the United States, J. Perform. Constr. Facil. 17 (2003) 144–150.
[2] A. Shirole, R. Holt, Planning for a Comprehensive Bridge Safety Assurance Program, Transportation Research Board 60th Annual Meeting, Transportation Research Board, Washington, DC, 1991, pp. 39–50.
[3] X. Yu, B. Zhang, J. Tao, X. Yu, A new time-domain reflectometry bridge scour sensor, Struct. Health Monit. 12 (2013) 99–113.
[4] G. Chen, B. Schafer, Z. Lin, Y. Huang, O. Suaznabar, J. Shen, Real-time Monitoring of Bridge Scour with Magnetic Field Strength Measurement, Transportation Research Board 92nd Annual Meeting, Transportation Research Board, Washington, DC, 2013, pp. 4235–4244.
[5] F. De Falco, R. Mele, The monitoring of bridges for scour by sonar and sedimetri, NDT E Int. 35 (2002) 117–123.
[6] J.-L. Briaud, S. Hurlebaus, K.-A. Chang, C. Yao, H. Sharma, O.-Y. Yu, C. Darby, B.E. Hunt, G.R. Price, Realtime Monitoring of Bridge Scour Using Remote Monitoring Technology, Texas Transportation Institute, Texas A&M University System, 2011, pp. 1–440.
[7] B. Wu, W. Chen, H. Li, Real-time Monitoring of Bridge Scouring Using Ultrasonic Sensing Technology, SPIE Smart Structures and Materials & Nondestructive Evaluation and Health Monitoring, International Society for Optics and Photonics, San Diego, CA, USA, 2012, pp. 1–9.
[8] A. Radchenko, D. Pommerenke, G. Chen, P. Maheshwari, S. Shinde, V. Pilla, Y.R. Zheng, Real Time Bridge Scour Monitoring with Magneto-Inductive Field Coupling, SPIE Smart Structures and Materials; Nondestructive Evaluation and Health Monitoring, International Society for Optics and Photonics, San Diego, CA, USA, 2013, pp. 1–15.
[9] G. Chen, D. Pommerenke, Z. Zhou, Y. Huang, A. Radchenko, Sensors for Integrated Monitoring and Mitigation of Erosion, Google Patents, USA, 2013.
[10] J. Tao, X. Yu, X. Yu, Real-time TDR Field Bridge Scour Monitoring System, Structures Congress, ASCE, Pittsburgh, USA, 2013, pp. 2996–3009.
[11] P. Dahal, D. Peng, Y.L. Yang, H. Sharif, RSS based bridge scour measurement using underwater acoustic sensor networks, Commun. Netw. 5 (2013) 641–648.
[12] C.W. Feng, H.Y. Huang, S.H. Ju, Integrating finite element method with GAs to estimate the scour depth of bridge, Int. J. Eng. Technol. 5 (2013) 462–465.
[13] K.-W. Liao, M.-Y. Cheng, Y.-F. Chiu, J.-H. Lee, Preliminary bridge health evaluation using the pier vibration frequency, Constr. Build. Mater. 102 (2016) 552–563.
[14] S. Li, S. He, H. Li, Y. Jin, Scour depth determination of bridge piers based on time-varying modal parameters: application to Hangzhou Bay bridge, J. Bridge Eng. 22 (2017) 1–13.
[15] L.J. Prendergast, D. Hester, K. Gavin, Determining the presence of scour around bridge foundations using vehicle-induced vibrations, J. Bridge Eng. 21 (2016) 1–14.
[16] J.L. Briaud, C. Yao, C. Darby, H. Sharma, S. Hurlebaus, G. Price, K. Chang, B. Hunt, O.Y. Yu, Motion Sensors for Scour Monitoring: Laboratory Experiments and Numerical Simulations, Transportation Research Board (TRB) 89th Annual Meeting, Transportation Research Board, Washington, DC, 2010, pp. 1–22.
[17] L.J. Prendergast, D. Hester, K. Gavin, J.J. O'Sullivan, An investigation of the changes in the natural frequency of a pile affected by scour, J. Sound Vib. 332 (2013) 6685–6702.
[18] X. Zhang, Y. Chen, W. Yao, Relationship between bridge natural frequencies and foundation scour depth based on IITD method, J. Appl. Sci. 6 (2013) 102–106.
[19] Y. Masui, O. Suzuki, Development of a soundness evaluation system for bridge substructured, JR East Tech. Rev. 14 (2009) 65–68.
[20] Y. Ko, W. Lee, W. Chang, H. Mei, C. Chen, Scour Evaluation of Bridge Foundations Using Vibration Measurement, 5th International Conference on Scour and Erosion, San Francisco, CA, USA, 2010, pp. 884–893.
[21] S. Ju, Determination of scoured bridge natural frequencies with soil-structure interaction, Soil Dynam. Earthq. Eng. 55 (2013) 247–254.
[22] T. Bao, R.A. Swartz, S. Vitton, Y. Sun, C. Zhang, Z. Liu, Critical insights for advanced bridge scour detection using the natural frequency, J. Sound Vib. 386 (2017) 116–133.
[23] L.J. Prendergast, K. Gavin, A comparison of initial stiffness formulations for small-strain soil-pile dynamic Winkler modelling, Soil Dynam. Earthq. Eng. 81 (2016) 27–41.
[24] A.B. Vesic, Beams on Elastic Subgrade and the Winkler's Hypothesis, Proceedings, 5th International Conference on Soil Mechanics and Foundation Engineering, Dunod, Paris, 1961, pp. 845–850.
[25] L.J. Prendergast, K. Gavin, D. Hester, Isolating the location of scour-induced stiffness loss in bridges using local modal behaviour, J. Civil Struct. Health Monitor. 7 (2017) 483–503.
[26] S.J. Oh, J.L. Briaud, K.A. Chang, H.C. Chen, Maximum Abutment Scour Depth in Cohesive Soils, Scour and Erosion, ASCE, 2010, pp. 132–141.
[27] D.S. Mueller, C.R. Wagner, Field Observations and Evaluations of Streambed Scour at Bridges, Research, Development, and Technology Turner-Fairbank Highway Research Center, US Department of Transportation, McLean, VA, 2005, pp. 1–137.
[28] I.P.O. Lam, Diameter Effects on P-Y Curves, Deep Foundations Institute, Hawthorne, New Jersey, 2013, pp. 1–15.
[29] L.F. Ling, Back Analysis of Lateral Load Test on Piles, Faculty of Engineering, University of Auckland, New Zealand, 1988.
[30] D.P. Carter, A Non-linear Soil Model for Predicting Lateral Pile Response, University of Auckland, New Zealand, 1984.
[31] S.A. Ashford, T. Juirnarongrit, Evaluation of pile diameter effect on initial modulus of subgrade reaction, J. Geotech. Geoenviron. Eng. 129 (2003) 234–242.
[32] T. Bao, Z. Liu, Vibration-based bridge scour detection: a review, Struct. Contr. Health Monit. 24 (2016) 1–19.
[33] H.Y. Huang, W.Y. Chou, S.H. Ju, C.W. Feng, Application of Finite Element Method and Genetic Algorithms in Bridge Scour Detection, Society for Social Management Systems Internet Journal, Society for Social Management Systems, Kochi, Japan, 2012.
[34] C. Yao, C. Darby, S. Hurlebaus, G. Price, H. Sharma, B. Hunt, O. Yu, K. Chang, J. Briaud, Scour Monitoring Development for Two Bridges in Texas, 5th International Conference on Scour and Erosion, Scour and Erosion, San Francisco, CA, USA, 2010, pp. 958–967.
[35] M. Shinoda, H. Haya, S. Murata, Nondestructive Evaluation of Railway Bridge Substructures by Percussion Test, Fourth International Conference on Scour and Erosion, The Japanese Geotechnical Society, Tokyo, Japan, 2008, pp. 285–290.
[36] L. Prendergast, K. Gavin, A review of bridge scour monitoring techniques, J. Rock Mech. Geotech. Eng. 6 (2014) 138–149.
[37] N. Lu, M. Kaya, Power law for elastic moduli of unsaturated soil, J. Geotech. Geoenviron. Eng. 140 (2013) 46–56.

[38] S. Foti, D. Sabia, Influence of foundation scour on the dynamic response of an existing bridge, J. Bridge Eng. 16 (2011) 295–304.
[39] P.K. Roy, N. Ganesan, Transient response of a cantilever beam subjected to an impulse load, J. Sound Vib. 183 (1995) 873–880.
[40] S.C. Dutta, R. Roy, A critical review on idealization and modeling for interaction among soil-foundation-structure system, Comput. Struct. 80 (2002) 1579–1594.
[41] Y.E. Mostafa, M.H.E. Naggar, Dynamic analysis of laterally loaded pile groups in sand and clay, Can. Geotech. J. 39 (2002) 1358–1383.
[42] S. Wang, B.L. Kutter, M.J. Chacko, D.W. Wilson, R.W. Boulanger, A. Abghari, Nonlinear seismic soil-pile structure interaction, Earthq. Spectra 14 (1998) 377–396.
[43] W. Versteijlen, A. Metrikine, K. van Dalen, A method for identification of an effective Winkler foundation for large-diameter offshore wind turbine support structures based on in-situ measured small-strain soil response and 3D modelling, Eng. Struct. 124 (2016) 221–236.
[44] R.R. Craig, A.J. Kurdila, Fundamentals of Structural Dynamics, John Wiley & Sons, New Jersey, 2006.
[45] API, Recommended Practice for Planning, Designing and Constructing Fixed Offshore Platforms-Working Stress Design, American Petroleum Institute, 2000.
[46] J. Atkinson, Non-linear soil stiffness in routine design, Geotechnique 50 (2000) 487–508.
[47] R. Luna, H. Jadi, Determination of Dynamic Soil Properties Using Geophysical Methods, the First International Conference on the Application of Geophysical and NDT Methodologies to Transportation Facilities and Infrastructure-Geophysics, 2000, pp. 1–15. ST. Louis, MO, USA.
[48] M. Pender, Discussion of "Evaluation of pile diameter effect on initial modulus of subgrade reaction, J. Geotech. Geoenviron. Eng. 130 (2004).
[49] G. Gazetas, Foundation vibrations, in: Foundation Engineering Handbook, Springer, 1991, pp. 553–593.
[50] K. Thieken, M. Achmus, K. Lemke, A new static p-y approach for piles with arbitrary dimensions in sand, Geotechnik 38 (2015) 267–288.
[51] W. Versteijlen, K. Van Dalen, A. Metrikine, L. Hamre, Assessing the Small-Strain Soil Stiffness for Offshore Wind Turbines Based on in Situ Seismic Measurements, Journal of Physics: Conference Series, IOP Publishing, 2014, pp. 1–10.
[52] J. Wiemann, K. Lesny, W. Richwien, Evaluation of the Pile Diameter Effects on Soil-Pile Stiffness, Proceedings of the 7th German Wind Energy Conference, 2004. Wilhelmshaven, Germany.
[53] S.P.H. Sørensen, L.B. Ibsen, A.H. Augustesen, Effects of Diameter on Initial Stiffness of Py Curves for Large-Diameter Piles in Sand, the European Conference on Numerical Methods in Geotechnical Engineering, CRC Press LLC, Trondheim, Norway, 2010, pp. 907–912.
[54] S.P.H. Sørensen, Soil-structure Interaction for Non-slender, Large-Diameter Offshore Monopiles, Department of Civil Engineering, Aalborg University Denmark, 2012.
[55] D. Kallehave, C.L. Thilsted, M. Liingaard, Modification of the API P-Y Formulation of Initial Stiffness of Sand, Offshore Site Investigation and Geotechnics: Integrated Technologies-Present and Future, Society of Underwater Technology, London, UK, 2012.
[56] G. Mylonakis, A. Nikolaou, G. Gazetas, Soil-pile-bridge seismic interaction: kinematic and inertial effects. Part I: soft soil, Earthq. Eng. Struct. Dyn. 26 (1997) 337–359.
[57] S. Cao, W. Yuan, Modified generalized pushover analysis for estimating longitudinal seismic demands of bridges with elevated pile foundation systems, Lat. Am. J. Solid. Struct. 11 (2014) 2696–2712.
[58] I. Paul C, Rizzo Associates, Elastic Modulus of Soil Layers, 2009.